Renewable Energy 34 (2009) 1765–1773

Contents lists available at ScienceDirect

Renewable Energy

journal homepage: www.elsevier.com/locate/renene

An analysis of a packed bed latent heat thermal energy storage system using PCM capsules: Numerical investigation

A. Felix Regin*, S.C. Solanki, J.S. Saini

Mechanical & Industrial Engineering Department, Indian Institute of Technology Roorkee, Roorkee 247 667, UA, India

ARTICLE INFO

Article history:
Received 26 January 2008
Accepted 9 December 2008

Keywords:
PCM capsule
Phase change material
Paraffin wax
Latent heat thermal energy storage
Solidification
Melting

ABSTRACT

This paper is aimed at analyzing the behavior of a packed bed latent heat thermal energy storage system. The packed bed is composed of spherical capsules filled with paraffin wax as PCM usable with a solar water heating system. The model developed in this study uses the fundamental equations similar to those of Schumann, except that the phase change phenomena of PCM inside the capsules are analyzed by using enthalpy method. The equations are numerically solved, and the results obtained are used for the thermal performance analysis of both charging and discharging processes. The effects of the inlet heat transfer fluid temperature (Stefan number), mass flow rate and phase change temperature range on the thermal performance of the capsules of various radii have been investigated. The results indicate that for the proper modeling of performance of the system the phase change temperature range of the PCM must be accurately known, and should be taken into account.

1. Introduction

Even though the problem of thermal energy storage within a capsule has been extensively studied, very little information is available on its performance in the case of latent heat thermal energy storage packed bed systems consisting of such capsules. The packed bed latent heat thermal energy storage systems have been used for applications such as, solar thermal energy storage, low temperature storage systems for central air conditioning, energy efficient buildings and waste heat recovery systems [1]. Such systems have the advantage of large surface to volume ratio of the packed beds and of higher storage density for the phase change materials compared to conventional bulk storage in tank heat exchangers and sensible heat storage systems. A storage system operates in three modes as follows.

1.1. Charging mode

The charging mode starts with circulation of the heat transfer fluid heated in the collection system at a temperature higher than the PCM melting temperature. This mode occurs during day time when solar energy collection takes place and terminates with complete melting of the PCM, charging of the store does not terminate with complete melting of the PCM if the inlet fluid temperature is above the melt temperature, charging of sensible heat continues.

1.2. Discharging mode

The discharging mode is started by circulation of the cold heat transfer fluid having inlet temperature lower than the PCM melting temperature. The heat transfer fluid exit temperature is time dependent because the rate of solidification of the PCM varies with time. This mode terminates with complete solidification of the PCM.

1.3. Stand by mode

This mode occurs when there is no further storage of energy occurring because of decreasing heat transfer fluid temperature or the storage tank is completely charged or the energy is directly fed to the utility without using storage and/or no heating from the bed is required. This is the transition period between the charge and discharge modes.

The major factors to be considered in the design of a storage unit containing a PCM include: (1) temperature limits within which the unit is to operate; (2) the thermophysical properties of the PCM; (3) the storage capacity of the tank; (4) the configuration of the storage

* Corresponding author. Tel.: +91 9818354268; fax: +91 1332 285665.
E-mail addresses: felixregin@gmail.com, felixregin@rediffmail.com (A. Felix Regin).

0960-1481/$ – see front matter © 2008 Elsevier Ltd. All rights reserved.
doi:10.1016/j.renene.2008.12.012

Nomenclature

A	surface area of capsule, m^2
C_p	specific heat, J/kg K
D	diameter of the bed, m
D_c	diameter of the capsule, m
$(\Delta T)_m$	solid–liquid phase change range, °C
$(\Delta T)_p$	solid–solid phase change range, °C
Δx	element thickness, m
H	specific enthalpy, J/kg
h	outer convective heat transfer coefficient, W/m^2 K
k	thermal conductivity of PCM, W/m K
k_c	thermal conductivity of capsule material, W/m K
L	latent heat of melting, J/kg
l	length of the bed, m
L_p	latent heat of solid–solid phase change, J/kg
m	mass of PCM, kg
$\dot{m}_f$	mass flow rate of heat transfer fluid
m_f	total mass of heat transfer fluid in the bed, kg
N	number of elements in the bed
Nu	Nusselt number
Q_{ch}	charged energy of the tank, kJ
Q_{dis}	discharged energy of the tank, kJ
Q_{total}	total energy storage capacity of the tank, kJ
Re	Reynolds number
R_{ext}	thermal resistance due to convection on the external surface of the capsule shell
R_c	thermal resistance due to conduction through the capsule wall
$R_{in}(t)$	resistance due to the solidified/melt PCM layer inside the capsule
Ste	Stefan number, $C_{pl}(T_f - T_m)/L$
T_b	bed temperature, °C
$\overline{T}_b$	average temperature of the bed, °C
$\overline{T}_c$	average temperature of capsules in the bed, °C
T_f	heat transfer fluid temperature, °C
$\overline{T}_f$	average heat transfer fluid temperature of the bed, °C
T_m	melting temperature, °C
T_p	solid–solid phase change temperature, °C
T_w	capsule wall temperature, °C
T_{final}	final temperature of the bed, °C
$T_{initial}$	initial temperature of the bed, °C
T_∞	environment temperature, °C
t	time, s
U_o	overall heat transfer coefficient of capsule, W/m^2 K
U_s	overall heat transfer coefficient of storage tank outer wall, W/m^2 K
U_v	overall volumetric heat transfer coefficient, W/m^3 K
$\overline{u}$	superficial velocity in the bed, m/s
X_l	melt fraction of the bed, %
X_s	solid fraction of the bed, %
X_t	total melt or solidified fraction of the bed, %
ρ_b	density of bed, kg/m^3
ρ_f	density of heat transfer fluid, kg/m^3
ε	porosity

Subscripts

B	bed
f	heat transfer fluid
l	liquid PCM
s	solid PCM

unit; (5) the type of heat transfer fluid and (6) pressure drop and pumping power.

It is generally reported in the literature that the first analytical study on modeling of the packed bed was conducted by Schumann [2] and most of the work reported till date has been focused on Schumann's model. Laybourn [3] predicted the heat transfer rates of cold storage tank during charging and discharging for building cooling applications with rectangular capsules using the concept of thermal resistance, which comprised of the convective resistance, wall resistance and ice layer resistance. Ismail and Henriquez [4] presented a mathematical model for predicting the thermal performance of the cylindrical storage tank containing spherical capsules filled with water as PCM. The model was used to investigate the influence of the working fluid entry temperature, the flow rate of the working fluid and material of the spherical capsule of 77 mm diameter during the solidification process. Arnold [5] has investigated the melting and freezing process of water as PCM within spherical capsules at macro- (storage tank) and micro- (single capsule) levels, separately and linking them by the heat transfer across the capsule wall. Bedecarrets et al. [6,7] have investigated the ice storage tank using spherical capsules. They took into account the supercooling phenomenon during solidification of water. The flow pattern inside the tank and the effects of the position of the tank, coolant flow rate and inlet temperature on the performance of cold storage have been discussed. Jotshi et al. [8] studied the thermophysical properties of Alum/Ammonium Nitrate Eutectic for solar space heating applications and investigated the performance of a packed bed system when the eutectic is encapsulated in 0.0254 m diameter high density polyethylene balls and concluded that the Stanton number empirical equation for a typical packed bed thermal system fails if there is a phase change in the bed material. Chen et al. [9–11] developed a one dimensional porous medium model and a lump model assuming temperature uniformity in packed capsules to determine the thermal performance of a low temperature storage system during the solidification process. Recently, Cho and Choi [12] and Goncalves and Probert [13] conducted experiments on the freezing and the melting of paraffin and $MgCl_2 \cdot 6H_2O$ respectively. Most of the aforementioned investigations do not consider the non-isothermal behavior of the phase change process.

The major objective of the present study is to investigate the effect of phase change temperature range on the performance of the packed bed latent heat thermal energy storage system consisting of spherical capsules for solar water heating applications. The effects of size of the capsules, inlet heat transfer fluid temperature and fluid flow rate have been discussed for charging and discharging processes.

2. Numerical analysis

Fig. 1 shows the layout of the physical system that has been investigated.

Assumptions involved in the present study are:

1. The tank is insulated and vertical with flow from the top when charging and flow from the bottom when discharging.
2. The flow in the tank is axial and incompressible.
3. The thermophysical properties of the heat transfer fluid are invariant with temperature.
4. The porosity of the bed, which is defined as the ratio of the void volume to the total volume of the packed bed, is 0.4 [14].

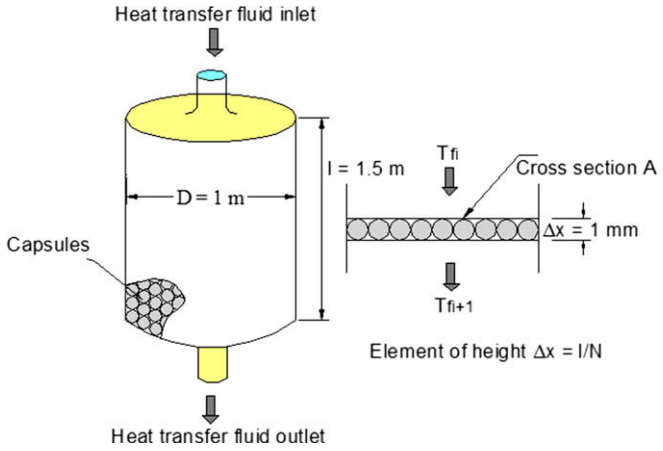

Fig. 1. Layout and details of the storage system.

5. Variation of temperature is only along the axial direction, i.e. the temperature is independent of radial position.
6. The tank of length l has been divided into N elements of sufficiently small length l/N so that the element can be assumed to be at a single temperature.
7. Radiant heat transfer between the capsules is negligible.
8. There is no internal heat generation in the bed.

The packed bed column is divided into N elements, each containing PCM capsules surrounded by heat transfer fluid. The energy balance on an element of volume $A\Delta x$ having PCM at a temperature T_b and the heat transfer fluid flowing at the rate of $\dot{m}_f$ and entering at a temperature T_f can be written as

$$(\dot{m}C_p)_f T_f - (\dot{m}C_p)_f\left[T_f + \frac{\partial T_f}{\partial x}\Delta x\right] = U_v A\Delta x\left(T_f - T_b\right) + U_s \pi D\Delta x\left(T_f - T_\infty\right) + \rho_f (A\Delta x)\varepsilon C_{p,f}\frac{\partial T_f}{\partial t} \quad (1)$$

The left hand side of Eq. (1) represents heat flow by the movement of heat transfer fluid. The first and second terms on the right hand side represent the heat exchange between the capsule and heat transfer fluid and heat loss to the environment respectively. The last term of Eq. (1) represents the rate of stored energy of the heat transfer fluid in the control volume.

In case, the heat losses can be neglected (the storage tank is considered to be well insulated) and the energy stored in the heat transfer fluid is negligibly small, the energy balance at an instance of time becomes.

$$(\dot{m}C_p)_f T_f - (\dot{m}C_p)_f\left[T_f + \frac{\partial T_f}{\partial x}\Delta x\right] - U_v A\Delta x\left(T_f - T_b\right) = 0 \quad (2)$$

or

$$\frac{\partial T_f}{\partial x} = \frac{-U_v A}{(\dot{m}C_p)_f}\left(T_f - T_b\right) \quad (3)$$

On simplification

$$\frac{\partial T_f}{\partial\left(x/l\right)} = -\mathrm{NTU}\left(T_f - T_b\right) \quad (4)$$

where NTU$[= (U_v A l)/((\dot{m}C_p)_f)]$ is the number of transfer units.

Integration yields

$$\frac{T_{fi+1} - T_{bi}}{T_{fi} - T_{bi}} = \exp\left(\frac{-\mathrm{NTU}}{N}\right) \quad (5)$$

or

$$\frac{T_{fi} - T_{fi+1}}{T_{fi} - T_{bi}} = 1 - \exp\left(\frac{-\mathrm{NTU}}{N}\right) \quad (6)$$

The outlet temperature of heat transfer fluid for ith element is:

$$T_{fi+1} = T_{fi} - \left[\left(T_{fi} - T_{bi}\right)\left(1 - \exp\left(\frac{-\mathrm{NTU}}{N}\right)\right)\right] \quad (7)$$

where T_{fi} is the heat transfer fluid temperature at inlet to the element, T_{fi+1} is the heat transfer fluid temperature at outlet from the element, T_{bi} represents the bed temperature of the element and $N = 1/\Delta x$ is the number of elements in the packed bed. Eq. (7) can be written for each control volume forming a system of N simultaneous equations. The NTU value and bed temperature of the element (T_{bi}) can be determined by knowing the volumetric heat transfer coefficient and the energy transferred into the PCM capsules. This can be explained as follows:

The volumetric heat transfer coefficient for thermal storage system can be written as [15]:

$$U_v = 6U_o(1-\varepsilon)/D_c \quad (8)$$

For the capsule, the outer surface overall heat transfer coefficient, U_o Eq. (8), is a function of the mode (either charging or discharging), the state of the PCM capsule in the control volume (fully liquid, fully solid, or phase change processes) and the mechanism of heat transfer (conduction, convection or combined conduction and convection).

During the fully liquid or fully solid stages, the overall heat transfer coefficient can be calculated by using thermal resistance concept for each capsule as given below:

$$U_o = (1/A)(R_{ext} + R_c)^{-1} \quad (9)$$

where R_{ext} is the convective thermal resistance on the external surface of the capsule shell and R_c is the conductive thermal resistance through the capsule wall.

During the phase change process the outer surface overall heat transfer coefficient can be calculated by using thermal resistance concept for each capsule as given below:

$$U_o = (1/A)(R_{ext} + R_c + R_{in}(t))^{-1} \quad (10)$$

where R_{ext} is the thermal resistance due to convection on the external surface of the capsule shell, R_c is the thermal resistance due to conduction through the capsule wall and $R_{in}(t)$ is the resistance due to the solidified/melt PCM layer inside the capsule. It is a function of time.

The external resistance R_{ext} between the capsule wall and the heat transfer fluid depends on the porosity of the bed, heat transfer fluid properties and the Reynolds number of the heat transfer fluid flow and can be determined from the Nusselt number correlation proposed by Wekaeo et al. [16] as

$$\mathrm{Nu}_{D_c} = 2.0 + 1.1[6(1-\varepsilon)]^{0.6}\mathrm{Re}_{D_c}^{0.6}\mathrm{Pr}_f^{1/3} \quad (11)$$

The Reynolds number Re_{D_c} can be obtained from the relation $\mathrm{Re}_{D_c} = \rho\bar{u}D_c/\mu$ where D_c is the capsule diameter and $\bar{u}$ is the superficial velocity in the bed.

The internal resistance of the capsule $R_{in}(t)$ depends on the solid–liquid interface position which can be calculated by using one dimensional heat conduction model with phase change as derived by the authors in references [17,18] for the solidification and

references [19,20] for melting of PCM inside cylindrical and spherical capsules respectively.

The bed temperature is calculated by using the energy balance between the heat transfer fluid and the bed. The energy transferred to the bed, $U_v A\Delta x(T_f - T_b)$, results in raising the bed temperature at the rate of dT_b/dt written as

$$U_v A\Delta x\left(T_f - T_b\right) = \rho_b(A\Delta x)(1-\varepsilon)C_{p,b}\frac{dT_b}{dt} \quad (12)$$

For simplification, multiply by $((Al)/(\dot{m}C_p)_f)$ on both sides

$$U_v\left(T_f - T_b\right)\left(\frac{Al}{(\dot{m}C_p)_f}\right) = (\rho C_p)_b(1-\varepsilon)\frac{dT_b}{dt}\left(\frac{Al}{(\dot{m}C_p)_f}\right) \quad (13)$$

Since NTU$[= (U_v Al)/((\dot{m}C_p)_f)]$, this equation can be written as

$$\frac{(\rho C_p)_b(1-\varepsilon)Al}{(\dot{m}C_p)_f}\frac{dT_b}{dt} = \mathrm{NTU}\left(T_f - T_b\right) \quad (14)$$

Eq. (14) can be discretized for '*i*th' element by using simple explicit and first order finite difference formulation [21], and can be written as

$$\frac{(\rho C_p)_b(1-\varepsilon)Al}{(\dot{m}C_p)_f}\frac{\left(T_{bi}^{n+1} - T_{bi}^{n}\right)}{\Delta t} = \mathrm{NTU}\left(T_{fi}^{n} - T_{bi}^{n}\right) \quad (15)$$

$$\left(T_{bi}^{n+1} - T_{bi}^{n}\right)(\rho C_p)_b(1-\varepsilon)Al = (\dot{m}C_p)_f\Delta t\cdot\mathrm{NTU}\left(T_{fi}^{n} - T_{bi}^{n}\right) \quad (16)$$

This energy balance equation can be applicable only to the sensible heat storage materials and can be converted to enthalpy equation that can be applicable to the phase change storage bed material as

$$\left(H_{bi}^{n+1} - H_{bi}^{n}\right)\rho_b(1-\varepsilon)Al = (\dot{m}C_p)_f\Delta t\cdot\mathrm{NTU}\left(T_{fi}^{n} - T_{bi}^{n}\right) \quad (17)$$

$$H_{bi}^{n+1} = \frac{1}{\rho_b(1-\varepsilon)Al}(\dot{m}C_p)_f\Delta t\cdot\mathrm{NTU}\left(T_{fi}^{n} - T_{bi}^{n}\right) + H_{bi}^{n} \quad (18)$$

Using this equation, enthalpy of bed in the element at particular time can be determined by using the known enthalpy values in the previous time period. This equation is valid at all elements at a particular time.

The phase change material used in this study is a technical grade Paraffin wax of congealing point 58–60 °C with a purity of 99%. For determining the behavior of the PCM during melting process the measurements have been performed with TA Instruments Differential Scanning Calorimeter (DSC) 2910 module with a liquid nitrogen cooling system. The DSC curve for melting of the paraffin wax is shown in Fig. 2. It is seen that there exist two peaks, the larger peak is due to solid–liquid phase change and the smaller peak due to solid–solid phase transition at about 10 °C below the main melting temperature range. The phase change process of paraffin wax can be divided into five sub-processes, i.e. solid phase, solid–solid phase change in temperature range, above the solid phase change temperature range but below the melting temperature range, solid–liquid phase change in temperature range and the liquid phase.

The corresponding enthalpy–temperature (*H*–*T*) relations are:

(i) When PCM is in solid phase:

$$H = C_{ps}T \quad T \le T_{(p-a_1)} \quad (19)$$

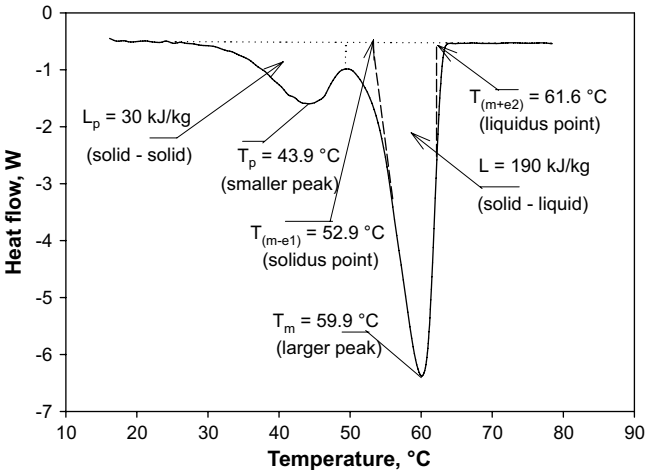

Fig. 2. DSC signal for the paraffin wax used.

(ii) When PCM is in solid–solid phase:

As the phase change occurs over a range of temperature $T_{(p-a_1)}$ to $T_{(p+a_2)}$ the enthalpy for the phase change is calculated by dividing the latent heat L_p for complete solid–solid phase change by the range of temperature and multiplied by the actual temperature change, i.e. $((L_p)/(a_1+a_2))(T - T_{(p-a_1)})$

$$H = C_{ps}T + \frac{L_p}{(a_1+a_2)}\left(T - T_{(p-a_1)}\right) \quad T_{(p-a_1)} < T < T_{(p+a_2)} \quad (20)$$

(iii) When PCM is in the above solid phase change temperature range but below the melting temperature range:

$$H = C_{ps}T + L_p \quad T_{(p+a_2)} \le T \le T_{(m-e_1)} \quad (21)$$

(iv) When PCM is in the solid–liquid phase:

This occurs in a temperature range $T_{(m-e_1)}$ to $T_{(m+e_2)}$, the latent heat L is similarly assumed to be supplied over this range and enthalpy is accordingly written as:

$$H = C_{ps}T + L_p + \frac{L}{(e_1+e_2)}\left(T - T_{(m-e_1)}\right) \quad T_{(m-e_1)} < T < T_{(m+e_2)} \quad (22)$$

(v) When PCM is in the liquid phase:

$$H = C_{ps}(T_m - T_{initial}) + C_{pl}\left(T_{final} - T_m\right) + L_p + L \quad T \ge T_{(m+e_2)} \quad (23)$$

The bed temperature T_b can be evaluated as a function of H_b, i.e. by employing the enthalpy as the dependent variable and temperature as the independent variable. The temperature distribution of all the elements in the bed is predicted at an instant of time by knowing the enthalpy values in each element. Temperature distribution of the bed as function of location of the storage tank

and time can indicate the amount of energy stored as well as the stratification in the bed.

The melt/solidified fraction of an element can be calculated based on the temperature of bed at a particular time. The total melt fraction or solidified fraction in a storage tank represented by integrating the melt/solidified fraction distribution in all the elements in the bed using the following equation:

$$X_t = \sum_{i=1}^{N} \frac{X_i}{N} \tag{24}$$

where X_t is the total melt or solidified fraction of the bed, X_i is the melt or solidified fraction of an element i and N is the total number of elements in the bed.

The total energy stored in the 'ith' element can then be expressed as the sum of the heat storage of capsules and the heat transfer fluid:

$$q_{\text{total},i} = q_{\text{PCM},i} + q_{\text{HTF},i} \tag{25}$$

The energy stored in the capsules contained in the bed element 'i' is given by

$$q_{\text{PCM},i} = \int_{T_{\text{initial}}}^{T_{p-a_1}} mC_{ps}\mathrm{d}T + \int_{T_{p-a_1}}^{T_{p+a_2}} mC_{ps}\mathrm{d}T + mL_p + \int_{T_{m-e_1}}^{T_{m+e_2}} mC_{pl}\mathrm{d}T + mL + \int_{T_{m+e_2}}^{T_{\text{final}}} mC_{pl}\mathrm{d}T \tag{26}$$

The energy stored in the heat transfer fluid is given by

$$q_{\text{HTF},i} = m_f C_{p,f}\left(T_{\text{initial}} - T_{\text{final}}\right) \tag{27}$$

where T_{initial} denotes the initial temperature, T_{final} the final temperature of the process and m_f is the mass of the heat transfer fluid in the element.

The energy stored in the storage comprising of 'N' such elements can then be written as:

$$Q_{\text{storage}} = \sum_{i=1}^{N} q_{\text{total},i} \tag{28}$$

Alternatively, the stored energy of the system while charging, Q_{ch} may be computed using the molten fraction of the PCM, temperature of the PCM and that of the heat transfer fluid inside the tank. Similarly the discharged energy of the system Q_{dis} may be computed using the solidified fraction of the PCM, temperature of PCM and that of the heat transfer fluid. These quantities can be written respectively, as:

$$Q_{ch} = X_m L + mC_{ps}(T_m - T_{\text{initial}}) + mC_{pl}(\overline{T}_c - T_m) + m_f C_{p,f}\left(\overline{T}_f - T_{\text{initial}}\right) \tag{29}$$

$$Q_{dis} = X_s L + mC_{pl}\left(T_{\text{final}} - T_m\right) + mC_{ps}(T_m - \overline{T}_c) + m_f C_{p,f}\left(T_{\text{final}} - \overline{T}_c\right) \tag{30}$$

3. Results and discussion

Key parameters of the analysis are the heat transfer fluid inlet temperature, mass flow rate, phase change temperature range and the radius of the capsule. In the present work a cylindrical storage tank of 1 m diameter and 1.5 m length (length to diameter ratio 1.5) completely filled with PCM capsules has been considered for the storage of energy collected by a solar collector system for a period of 6 h per day. The storage system contains paraffin wax as phase change material in HDPE spherical capsule, having the storage capacity of 85.5 MJ of thermal energy when considering only the latent heat of the storage material. The total storage capacity of the tank increases to 143.7 MJ when considering the latent heat and sensible heat of the paraffin wax along with the sensible heat of the heat transfer fluid (water) over the temperature range of 20 °C. Numerical calculations were made with various element and time step sizes and it was found that the results are independent of element and time step size below respective sizes of 1 mm and 1 s. Consequently, these values were used in all numerical simulations.

Table 1 summarizes the range of operating parameters of this investigation. The results obtained from the analysis are presented and discussed below.

3.1. Temperature distribution of the bed

The temperature distribution of the bed was predicted with various values of Stefan number, mass flow rate, capsule diameter and PCM melting temperature range both for melting and solidification process. Fig. 3 shows typical temperature distribution of bed at different axial positions for various values of instant of time from start of the charging mode of 40 mm capsules. The flow rate is 0.0796 kg/s (~0.1 mm/s), and the initial temperature of the storage and the inlet temperature of heat transfer fluid are 50 °C and 70 °C respectively. During initial heating period, the capsules near the entrance are charged while those near the exit are very close to the initial bed temperature. As time elapses the bed temperature rises.

During the melting process there are three stages namely; solid heating, phase change and liquid heating as indicated in Fig. 3. The paraffin wax used in this experiment is characterized by melting in a range of temperature; the melting starts at a temperature of 52.9 °C ($T_{(m-e1)}$ in Fig. 3) and is completed at 61.6 °C ($T_{(m+e2)}$ in Fig. 3). The solid heating takes place up to the temperature $T_{(m-e1)}$ (stage 1 in Fig. 3), the phase change is between the range $T_{(m-e1)}$ to $T_{(m+e2)}$ (stage 2 in Fig. 3) and the liquid heating takes place above the temperature $T_{(m+e2)}$ (stage 3 in Fig. 3).

Fig. 4 shows the temperature distribution during solidification mode for a 40 mm capsule. These distributions also show characteristics similar to those of melting, i.e. liquid cooling (stage 1 in Fig. 4), solid cooling (stage 3 in Fig. 4) and solidification (stage 2 in Fig. 4). It can be observed that the bed is not completely solidified even at the end of 10 h where as almost the entire bed had melted in a much shorter period. This is due to the very low heat transfer coefficient during solidification process as compared to that of the melting process. It is because of high resistance of solidified layer formed in the inner wall of the capsule during solidification process, which reduces the heat transfer rate between the bed and the heat transfer fluid where as during melting process, the melted

Table 1
Range of operating parameters.

Problem	Initial temperature, °C	Stefan number, Ste (T_{HTF}, °C)	Mass flow rate, kg/s	Capsule radii, mm	Phase change temperature range, °C
Melting	50	0.1143–0.2051 (70–82 °C)	0.0398–0.1592	20–60	0–8.7
Solidification	70	0.1042–0.2621 (50–35 °C)	0.0398–0.1592	20–60	0–8.7

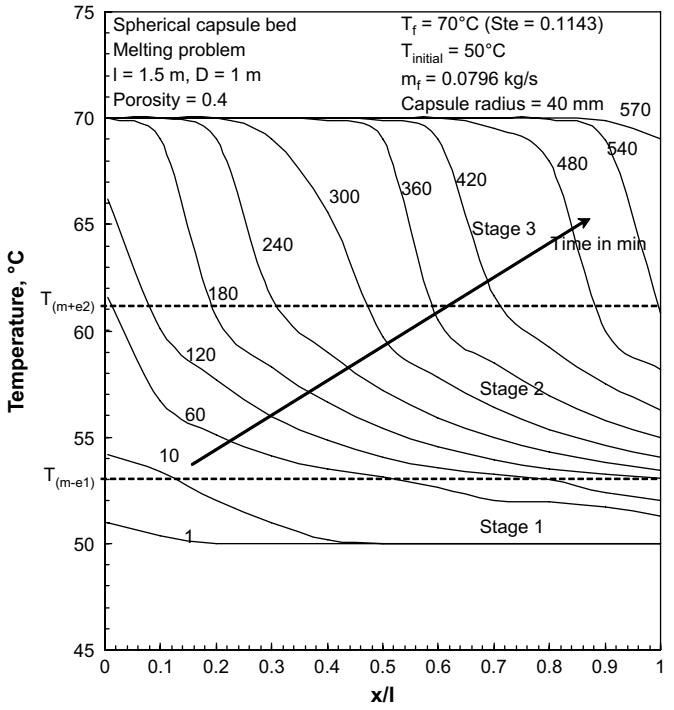

Fig. 3. Temperature profiles of melting of spherical capsules in the bed.

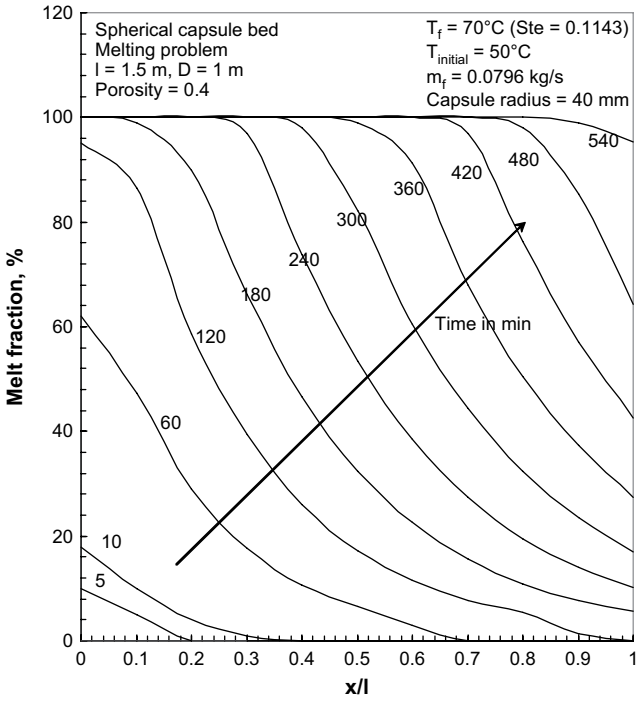

Fig. 5. Melt fraction distribution of the spherical capsule bed as function of time.

layer formed near the inner wall of the capsule increases the heat transfer rate by natural convection mode.

3.2. Melt/solid fraction distribution of the bed

Fig. 5 shows the melt fraction distribution of the bed as function of time and axial position during the charging mode of 40 mm capsules. It is observed high energy transfer in the inlet region leads to higher melt fraction there and the heat transfer fluid leaving the bed almost at the initial bed temperature leading to almost zero melt fraction. Fig. 6 shows the solid fraction distribution of the bed during the discharging mode.

3.3. Effect of heat transfer fluid temperature (or Stefan number)

Fig. 7 shows the total melt fraction of the PCM in the bed for various values of Stefan number (heat transfer fluid temperatures). The time to reach the complete melting of bed (melt fraction of

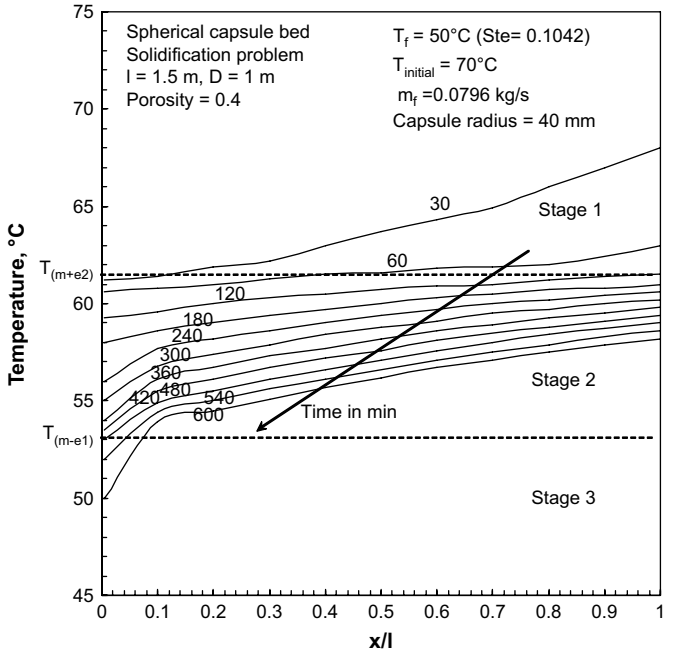

Fig. 4. Temperature profiles of solidification of spherical capsules in the bed.

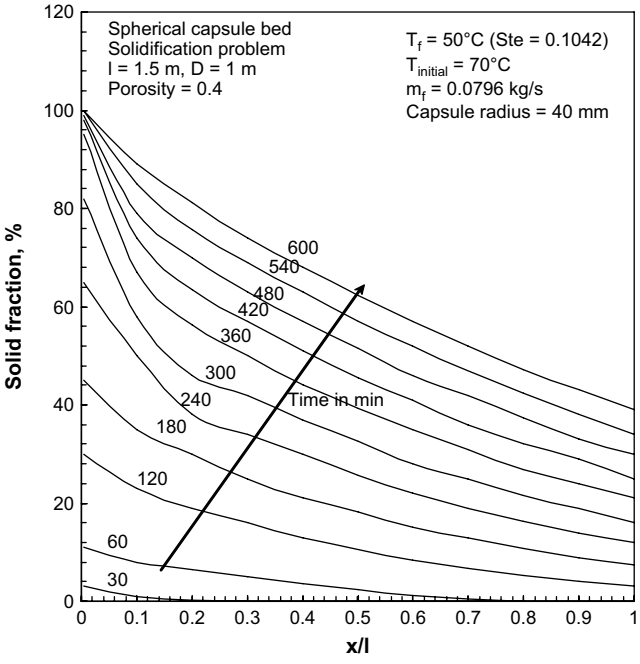

Fig. 6. Solid fraction distribution of the spherical capsule bed as a function of time.

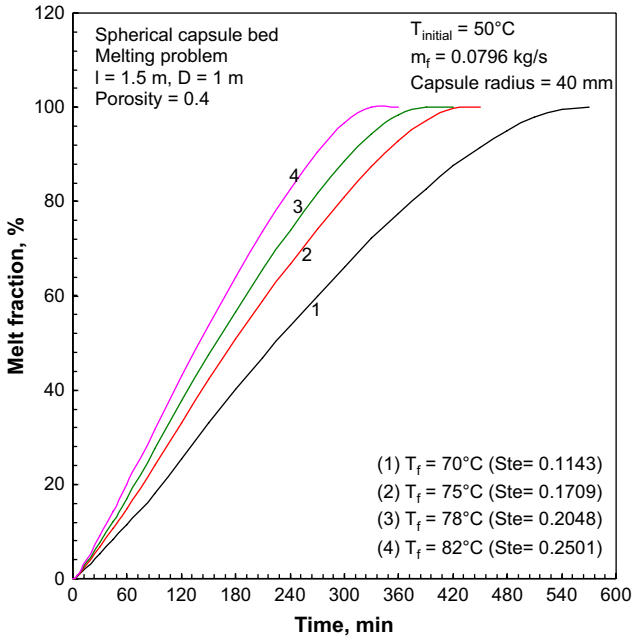

Fig. 7. Effect of Stefan number on melt fraction of the bed.

100%) decreases as the inlet temperature of heat transfer fluid is increased. For the Stefan number of 0.2501 ($T_{in} = 82\ ^{\circ}C$), the time was shorter by about 42% to reach the melt fraction of 100% than that for the Stefan number of 0.1143 ($T_{in} = 70\ ^{\circ}C$). This shows the melt fraction and the complete charging time are strongly affected by the inlet temperature of heat transfer fluid (Stefan number). Higher Stefan number (i.e. higher inlet heat transfer fluid temperature), the shorter the time interval for complete charging.

3.4. Effect of mass flow rate of heat transfer fluid

Fig. 8 shows the variation of total melt fraction of PCM as a function of time for different heat transfer fluid mass flow rates.

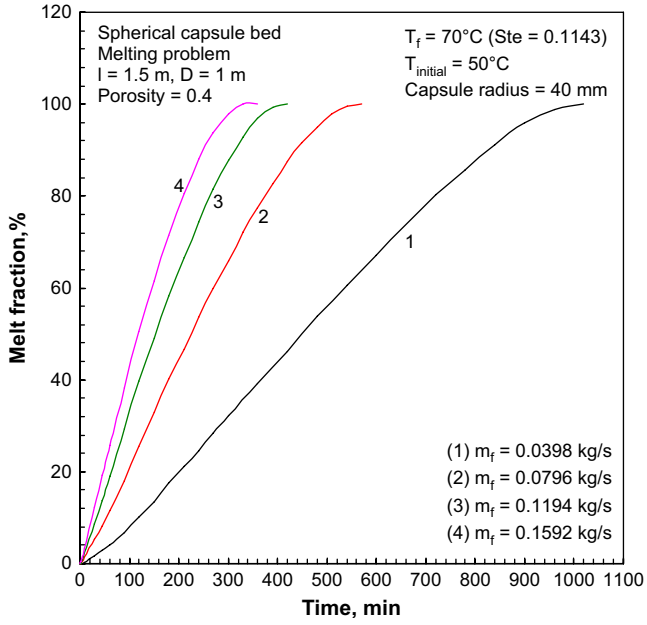

Fig. 8. Melt fraction vs time for various mass flow rate.

The curves rise to the complete melting position early with the increase in the mass flow rate. Higher the mass flow rate, the shorter the time interval needed for complete charging.

3.5. Effect of capsule size

Fig. 9 shows the total melt fraction of PCM as a function of capsule radius and time indicating the complete charging time of the bed is 480, 510, 540, 570, 600 and 630 min for 20, 25, 30, 40, 50 and 60 mm capsule radii respectively; the bed with smaller capsules taking less time for charging. It can be seen that at the end of 6 h of charging, the total melt fraction for 20 mm capsule is 80.2% and for 60 mm capsule is 73%. For the capsule of 20 mm radius it took shorter time by 24% to reach the melt fraction of 100% than that for the 60 mm capsule during the melting process.

Fig. 10 shows the total solidified fraction of PCM as a function of capsule radii. It can be observed that at the end of 6 h of discharging process the solidified fraction for 20 mm capsule is 51% while for 60 mm capsule is 26%; a reduction in solidification fraction of about 49%. For melting process, the effect of radius of capsule is much weaker, for example there is reduction of only 9% as the capsule radius changes from 60 mm to 20 mm. It means it is better to select a capsule of smaller radius to get higher storage rate in the bed.

3.6. Effect of melting temperature range on the performance of the system

Fig. 11 shows the temperature distribution in the storage tank for the melting of PCM at constant temperature process ($T_m = 59.9\ ^{\circ}C$). In the beginning, the PCM in the capsules near the entrance is heated and melted but the PCM in the capsules near the exit remains unaffected and the temperature is equal to the initial bed temperature. It requires a large amount of energy in terms of latent heat at a particular temperature for phase change process. The temperature of the bed is equal to the melting temperature of the PCM for longer period in this ideal case. A very high slope of temperature distribution is observed near the melting temperature

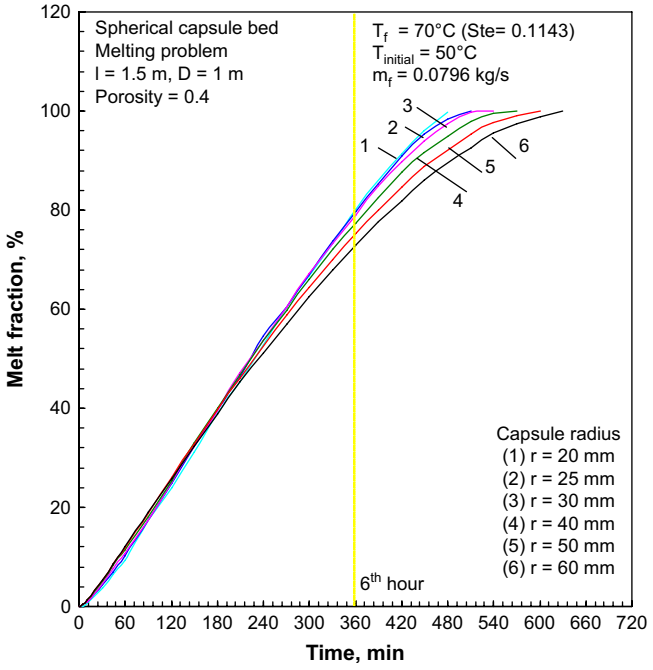

Fig. 9. Melt fraction of the spherical capsule bed for various capsule radii.

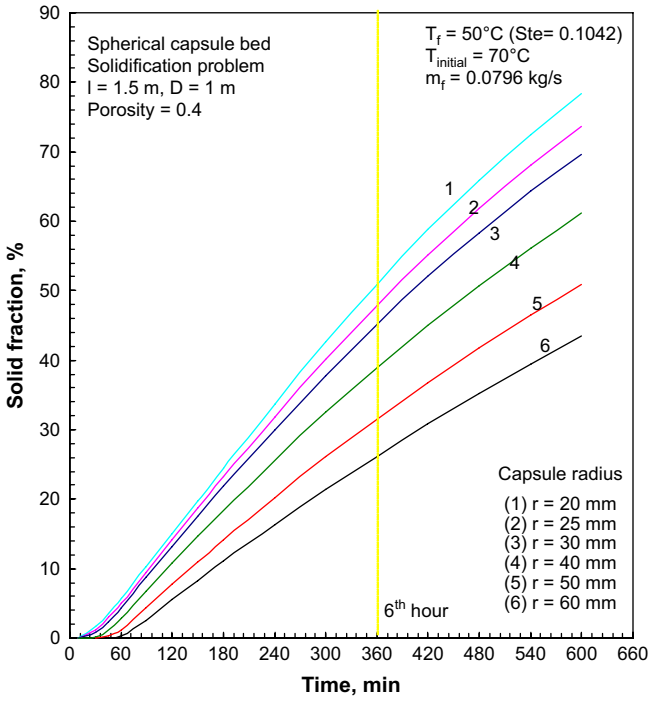

Fig. 10. Solid fraction of the spherical capsule bed for various capsule radii.

($T_m = 59.9\,^{\circ}C$) when melting is complete again a very high slope of temperature occurs near the inlet temperature of heat transfer fluid line. The charging of the capsule takes place by sensible heating of the solid and sensible heating of the liquid in the stage 1 and stage 2 of Fig. 11 respectively. For example, at x/l of 0.5, the bed takes 50 min to reach the melting temperature (solid heating), the bed is at the same temperature till 400 min during this period of 350 min the melting takes place at the melting temperature and finally the bed took 100 min to reach the temperature of 70 °C (liquid heating).

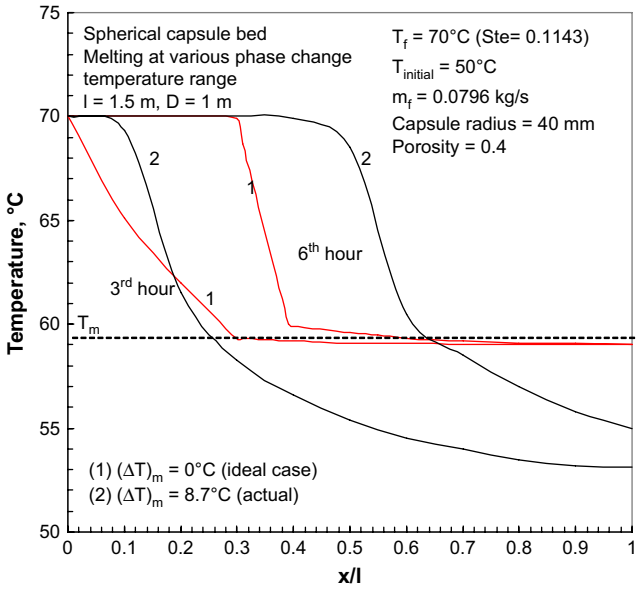

Fig. 12. Bed temperature profile at the end of 3rd and 6th hours of melting of spherical capsule at phase change temperature ranges of 0 and 8.7 °C.

The effect of phase change temperature range on the charging process is shown in Fig. 12 where the bed temperature profile at the end of 2nd, 4th and 6th hours of melting is shown for the case of PCM melting at fixed temperature of 59.9 °C and that melting in the temperature range $T_{(m-e_1)}$ to $T_{(m+e_2)}$. Higher stratification is observed for the PCM melting in the range of phase change (i.e. 8.7 °C) compared to that melting at a fixed temperature. This is because of higher heat transfer rate, since the PCM starts to melt at 52 °C which is much lower temperature as compared to 59.9 °C.

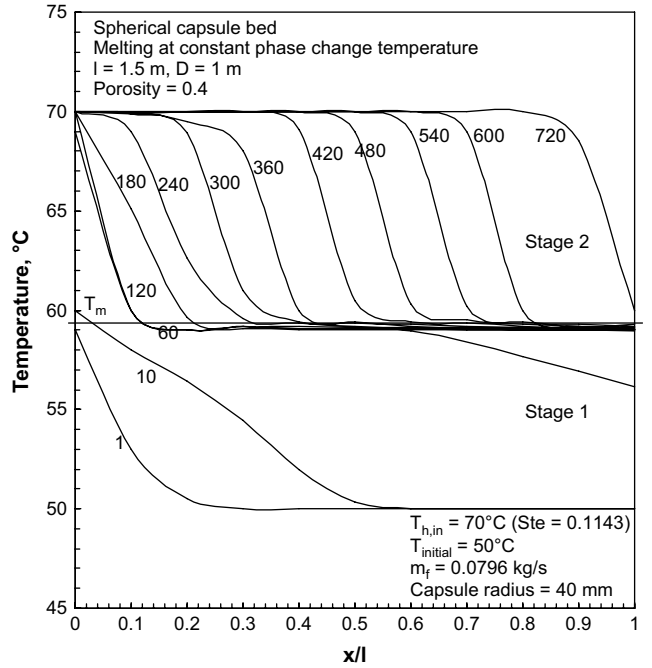

Fig. 11. Temperature distribution of melting of spherical capsule bed (melting at constant phase change temperature, $T_m = 59.9\,^{\circ}C$).

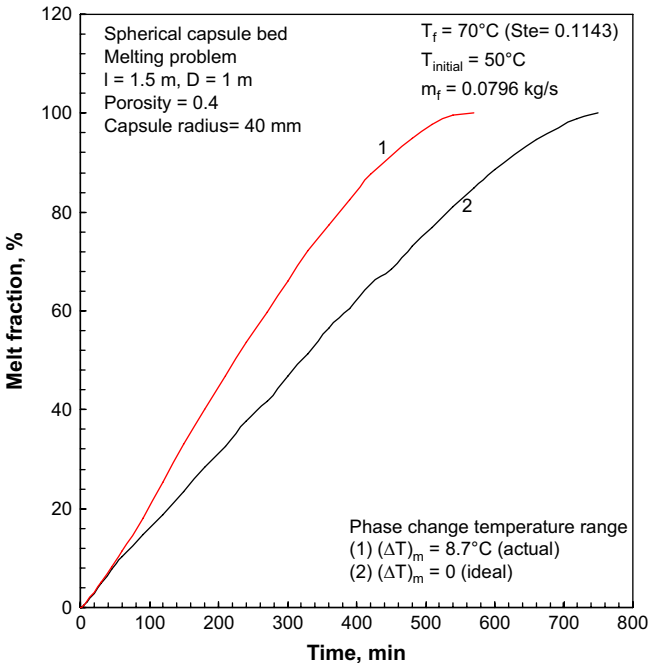

Fig. 13. Effect of phase change temperature range on melt fraction of the spherical capsule bed.

Even though the heat transfer coefficient is same in both the cases, the varying temperature difference between the PCM and heat transfer fluid, a different heat transfer rate is obtained. As a result, the bed having PCM melting in a temperature range reaches the complete melting earlier than the PCM with fixed melting temperature as can be seen in Fig. 13, which shows the total melt fraction as function of time for these time cases. A difference of 31.6% in the complete melting time for PCM with fixed phase change temperature and that with phase change in a temperature range ($(\Delta T)_m = 8.7\ ^\circ C$) is observed.

4. Conclusions

A model for a packed bed latent heat thermal energy storage using spherical capsules is developed in the present study to predict the thermal behavior of the system. This study investigates the effects of heat transfer fluid inlet temperature, mass flow rate, phase change temperature range and the radius of the capsule on the dynamic response of a packed bed latent heat thermal energy storage system using spherical capsules for both charging and discharging modes. The following conclusions can be drawn:

1. The complete solidification time is too longer compared to the melting time. This is due to the very low heat transfer coefficient during solidification.
2. Higher the Stefan number (i.e. higher inlet heat transfer fluid temperature) the shorter is the time for complete charging. Similarly for higher the mass flow rate of heat transfer fluid shorter is the time for complete charging.
3. The charging and discharging rate are significantly higher for the capsule of smaller radius compared those of larger radius.
4. The phase transition temperature range reduces the complete melting time; a difference of 31.6% is observed for the case when the PCM has melting in the temperature range as compared to that for a PCM with melting at fixed temperature.

References

[1] Felix Regin A, Solanki SC, Saini JS. Heat transfer characteristics of thermal energy storage system using PCM capsule: a review. Renewable and Sustainable Energy Reviews 2008;12:2438–58.
[2] Schumann TEW. Heat transfer: a liquid flowing through a porous prism. Journal of the Franklin Institute 1929;208:405–16.
[3] Laybourn DR. Thermal energy storage with encapsulated ice. ASHRAE Transactions 1988;94:1971–88.
[4] Ismail KAR, Henriquez JR. Numerical and experimental study of spherical capsules packed bed latent heat storage system. Applied Thermal Engineering 2002;22:1705–16.
[5] Arnold D. Dynamic simulation of encapsulated ice stores, part 1 – the model. ASHRAE Transactions 1996;96:1103–10.
[6] Bedecarrets JP, Strub F, Falcon B, Dumas JP. Phase change thermal energy storage using spherical capsules: performance of a test plant. International Journal of Refrigeration 1996;19:187–96.
[7] Kousksou T, Bedecarrets JP, Dumas JP, Mimet A. Dynamic modeling of the storage of an encapsulated ice tank. Applied Thermal Engineering 2005;25:1534–48.
[8] Jotshi CK, Hsieh CK, Goswami DY, Klausner JF, Srinivasan N. Thermal storage in ammonium alums/ammonium nitrate eutectic for solar space heating applications. Transactions of the ASME – Journal of Solar Energy Engineering 1998;120:20–4.
[9] Chen SL, Yue JS. A simplified analysis for cold storage in porous capsules with solidification. ASME Journal of Energy Resources and Technology 1991;113:108–16.
[10] Chen SL, Yue JS. Thermal performance of cool storage in packed capsules for air conditioning. Heat Recovery Systems & CHP 1991;11:551–61.
[11] Chen SL. One dimensional analysis of energy storage in packed capsules. ASME Journal of Solar Energy Engineering 1992;114:127–30.
[12] Cho Keumnam, Choi SH. Thermal characteristics of paraffin in a spherical capsule during freezing and melting process. International Journal of Heat and Mass Transfer 2000;43:3183–96.
[13] Goncalves LCC, Probert SD. Thermal energy storage: dynamic performance characteristics of cans each containing a phase change material, assembled as a packed bed. Applied Energy 1993;45:117–55.
[14] Yogi Goswami D, Kreith Frank, Kreider Jan F. Principle of solar engineering. Taylor & Francis Publication; 1999.
[15] Chandra P, Willits DH. Pressure drop and heat transfer characteristics of air-rockbed thermal storage systems. Solar Energy 1981;27:547–53.
[16] Wakao N, Kaguei S, Funazkri. Effect of fluid dispersion coefficients on particle to fluid heat transfer coefficients in packed beds. Chemical Engineering Science 1979;34:325–36.
[17] Felix Regin A, Solanki SC, Saini JS. Solidification of phase change materials inside a cylindrical capsule. In: Proceedings of ASME–ISHMT heat and mass transfer conference, IIT Guwahati, India; 2006.
[18] Felix Regin A, Solanki SC, Saini JS. Thermal performance analysis of phase change material capsules. In: Proceedings of international solar energy conference (ISES/ASES-2005), Florida, USA; 2005.
[19] Felix Regin A, Solanki SC, Saini JS. Latent heat thermal energy storage using cylindrical capsule: numerical and experimental investigations. Renewable Energy 2006;31:2025–41.
[20] Felix Regin A, Solanki SC, Saini JS. Experimental and numerical analysis of melting of PCM inside a spherical capsule. In: 9th AIAA/ASME joint thermophysics and heat transfer conference, paper no. AIAA-2006-3618, 7th June 2006, USA; 2006.
[21] Ozisik MN. Finite difference methods in heat transfer. CRC Press; 1994.